Fermi surface in the superconducting β-pyrochlore oxide $CsOs_2O_6$

T. Terashima (寺嶋太一) and S. Uji (宇治進也)
National Institute for Materials Science, Tsukuba, Ibaraki 305-0003, Japan

Y. Nagao (長尾洋平), J. Yamaura (山浦淳一), and Z. Hiroi (廣井善二)
Institute for Solid State Physics, University of Tokyo, Kashiwa, Chiba 277-8581, Japan

H. Harima (播磨尚朝)
Department of Physics, Graduate School of Science, Kobe University, Kobe, Hyogo 657-8501, Japan
(Received 22 October 2007; revised manuscript received 10 January 2008; published 15 February 2008)

We report de Haas–van Alphen effect (dHvA) measurements and band-structure calculations for $CsOs_2O_6$. Sixteen dHvA frequency branches are observed in the $(\bar{1}10)$ plane. The Fermi surface consists of hole and electron surfaces. The topology of the measured Fermi surface can be described by the band-structure calculations if slight rigid band shifts are incorporated. The electron surface has through holes in the $\langle 111 \rangle$ directions, indicating that the van Hove singularity is above the Fermi level unlike previously thought. Using band-structure results, we have estimated that the Stoner enhancement factor $S \sim 3.1$ and that the Wilson ratio $R \sim 0.86$. The dHvA effective masses are mostly between three and four times the corresponding band masses, which is consistent with the specific-heat mass enhancement of 3.6. We have also estimated the orbital-specific Stoner enhancement factor for one orbit from dHvA data: the most probable value of the product Sg, where g is the g factor, for that orbit is found to be 9.374. The small Wilson ratio and Stoner enhancement indicate rather limited importance of electron-electron interactions in $CsOs_2O_6$.

DOI: 10.1103/PhysRevB.77.064509 PACS number(s): 74.70.Dd, 71.18.+y, 71.20.Ps

I. INTRODUCTION

The search for and the study of superconducting transition-metal oxides are certainly one of the most active areas in solid state physics. The β-pyrochlore osmium oxides AOs_2O_6 (A=K, Rb, and Cs) joined the superconducting oxides club recently:[1–4] the superconducting transition temperature T_c=9.6, 6.3, and 3.3 K for A=K, Rb, and Cs, respectively. They crystallize in cubic structures with the space group $Fd\bar{3}m$ (No. 227),[5,6] and the primitive cell contains 2 f.u. The OsO_6 octahedra, sharing vertices, form a three-dimensional network, while the alkali ions are located in cages surrounded by the octahedra.

The Sommerfeld coefficient γ of the specific heat is 70 mJ/K^2 mol for A=K (Ref. 7) and 40 mJ/K^2 mol for A=Rb and Cs.[8,9] These values are approximately seven and four times larger than predicted by band-structure calculations,[10–13] indicating moderately strong mass renormalization due to many-body interactions. Whether the interactions are of electronic origin or of phononic origin is an important question and is, of course, intimately related to the mechanism of the superconductivity.

Originally, possible importance of electron correlations and of geometrical frustration inherent in the pyrochlore lattice was suggested.[1,14] The T^2 dependence of electrical resistivity, which is usually ascribed to electron-electron collisions, has been reported for the Rb and Cs compounds,[2,3] and also lately for the K compound.[15] A high pressure study[16] has shown that, for the Rb and Cs compounds, the coefficient of the T^2 term, which is a measure of the strength of electron-electron interactions, peaks when T_c reaches a maximum as a function of pressure. This might, indeed, indicate that the electron correlations play a role in the superconducting pairing mechanism. A muon spin rotation experiment[17] has suggested the possibility of an anisotropic order parameter, in favor of electronic scenarios of the superconductivity.

On the other hand, it has been pointed out that the potential energy associated with the displacement of an alkali ion in the cage is anharmonic, more or less flat near the equilibrium position,[11] which will allow the "rattling" motion[18] of the alkali ions. This is clearly manifested in the unusually large atomic displacement factors of the alkali ions found in x-ray[5,19] as well as neutron[6] structural analyses. Further, analyses of specific heat data require the inclusion of low-energy Einstein modes, which are most likely attributed to the rattling vibrations.[7,8,20] Since the anharmonicity grows rapidly in the sequence A=Cs, Rb, and K, the large variation of T_c among these otherwise similar compounds might be rooted in varying strength of electron–rattling-phonon interactions among them.[11] A rattling-phonon mediated strong-coupling scenario for the superconductivity has been proposed from detailed analyses of thermodynamic and transport data.[7]

In this paper, we report results of de Haas–van Alphen (dHvA) measurements and band-structure calculations for $CsOs_2O_6$. We determine the detailed shape of the Fermi surface by comparing the measured angular dependence of dHvA frequencies with band-structure predictions. We also estimate orbital-specific as well as bulk (Fermi-surface averaged) mass enhancements and Stoner enhancements, and consider the strength of electron correlations in $CsOs_2O_6$.

II. SAMPLE, EXPERIMENTS, AND BAND-STRUCTURE CALCULATIONS

The single-crystal sample of $CsOs_2O_6$ used for the dHvA measurements (Fig. 1) was taken from a batch of crystals prepared in a way similar to that described in Ref. 7. Very

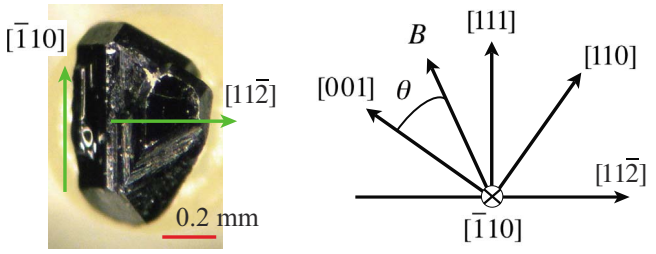

FIG. 1. (Color online) Sample and definition of the field angle. The approximate size of the sample is $0.8\times0.5\times0.6$ mm^3, and the top surface is the (111) plane. The magnetic field B was rotated in the $(\bar{1}10)$ plane, and the field angle θ is measured from the [001] axis. The axis of the pickup coil is parallel to [111].

high quality crystals can be grown in this way as evidenced by a large residual resistivity ratio of 750 observed in another crystal from the present growth batch.[21] The crystal axes of the sample were determined by x-ray diffraction.

dHvA oscillations were measured with the field-modulation technique.[22] The modulation frequency and amplitude were $f=67$ Hz and $b=0.01$ T, respectively. The detection was made at the second harmonic of the modulation frequency. The sample was placed in a pickup coil with the [111] axis parallel to the coil axis. The magnetic field B was rotated in the $(\bar{1}10)$ plane, and the field angle θ is measured from the [001] axis (Fig. 1). The same setup was used to measure ac magnetic susceptibility.

The dHvA magnetization oscillation M_{osc} due to an extremal cyclotron orbit normal to B enclosing the k-space area A is given by[22]

$$M_{osc}=-\sum_{r=1}^{\infty}a_r\sin\left[2\pi r\left(\frac{F}{B}-\frac{1}{2}\right)\pm\frac{\pi}{4}\right], \tag{1}$$

where

$$a_r=u\frac{FB^{1/2}}{\mu^*|A''|^{1/2}}r^{-3/2}R_{T,r}R_{D,r}R_{s,r}, \tag{2}$$

$$R_{T,r}=\frac{rK\mu^*T/B}{\sinh(rK\mu^*T/B)}, \tag{3}$$

$$R_{D,r}=\exp(-rK\mu^*x_D^*/B), \tag{4}$$

$$R_{s,r}=\cos\left(r\frac{\pi}{2}Sg\frac{m_{band}}{m_e}\right). \tag{5}$$

The frequency F is given by $F=(\hbar/2\pi e)A$. Not only the fundamental frequency F but also its harmonics ($r>1$) appear in M_{osc}. The $\pm$ sign in Eq. (1) depends on whether the orbit is minimal (+) or maximal (−). The constant u is positive. The effective mass m^* is enhanced over the band mass m_{band} by electron-electron and electron-phonon interactions, and μ^* is defined to be m^*/m_e, where m_e is the free electron mass. Similarly, other asterisked symbols indicate renormalized quantities. $|A''|$ is the curvature factor: $A''=\partial^2A/\partial\kappa^2$, where κ is the wave number along B. $R_{T,r}$ is the thermal damping factor, where K is a constant (14.69 T/K). The Dingle factor $R_{D,r}$ describes the influence of disorder or impurity scattering, x_D^* being the Dingle temperature. We can determine m^* and x_D^* by fitting $R_{T,r}$ and $R_{D,r}$ to T and B dependences of experimental oscillation amplitudes at constant B and T, respectively. We may also calculate the mean free path $l=\tau^*v_F^*$ of electrons from F, m^*, and x_D^* by using the formula, $A=\pi k_F^2$, $\hbar k_F=m^*v_F^*$, and $\tau^*=\hbar/2\pi k_Bx_D^*$, where k_B is the Boltzmann constant and τ^* the relaxation time of electrons. The spin-splitting factor $R_{s,r}$ is due to the interference between oscillations from up- and down-spin electrons. S is the Stoner enhancement factor, and g the electron g factor.

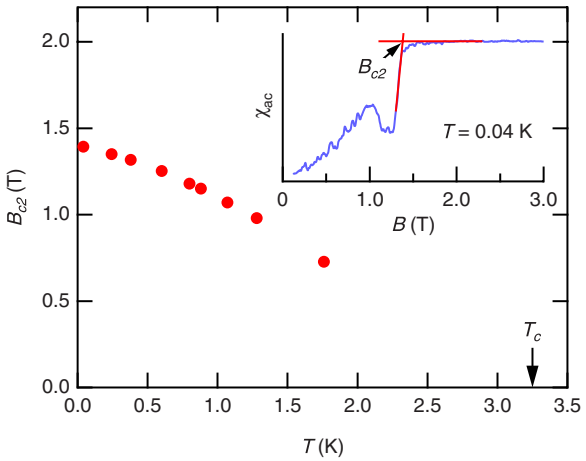

FIG. 2. (Color online) Upper critical field B_{c2} as a function of T. The inset shows ac magnetic susceptibility χ_{ac} against B and explains the determination of B_{c2}.

As a modulation field $b\cos(\omega t)$, where $\omega=2\pi f$, is applied parallel to B, the voltage v is induced in a pickup coil. Since Eq. (1) is nonlinear in B, it contains harmonics of ω. If the axis of the pickup coil is at an angle ϕ to B,[22]

$$v=\left(\cos\phi-\frac{1}{F}\frac{dF}{d\phi}\sin\phi\right)\sum_{k=1}^{\infty}v_k\sin(k\omega t). \tag{6}$$

The voltage v_k is given by

$$v_k=-\sum_{r=1}^{\infty}v_{k,r}\sin\left[2\pi r\left(\frac{F}{B}-\frac{1}{2}\right)\pm\frac{\pi}{4}-\frac{k\pi}{2}\right], \tag{7}$$

with

$$v_{k,r}=-2c\omega kJ_k(r\lambda)a_r. \tag{8}$$

c is a coupling constant of the pickup coil, J_k the Bessel function of the first kind of order k, and $\lambda=2\pi Fb/B^2$. With the present setup, $k=2$ (second-harmonic detection) and $\phi=\theta-54.7°$. Note that λ increases with decreasing B for a given b and that $J_2(\lambda)$ varies as $\sim\lambda^2$ for $\lambda\ll1$. Accordingly, dHvA oscillations with small frequencies (F) are often easier to observe at moderately low fields.

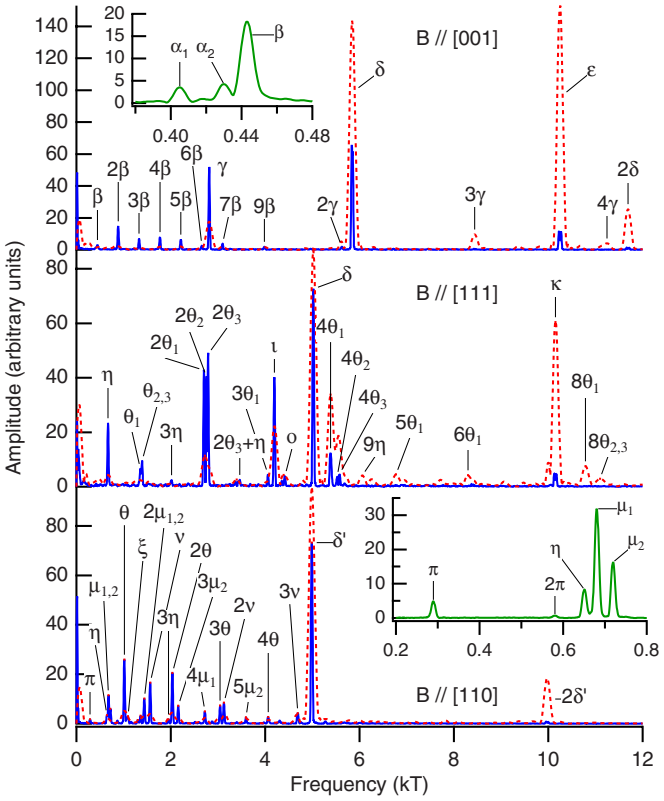

FIG. 3. (Color online) Fourier spectra of dHvA oscillations in $CsOs_2O_6$ at $T=0.05$ K for the high symmetry directions. The field ranges used are $7<B<13.9$ T (solid lines) and $14<B<17.5$ T (dotted lines). Fundamental frequencies are labeled with Greek letters, and "2β," "3β," etc., indicate the second and third harmonics of β, and so on. The insets show the spectra of long field sweeps especially performed to resolve finely spaced low frequencies: $3<B<17.5$ T for [001] and $4<B<17.5$ T for [110].

The electronic band-structure of $CsOs_2O_6$ was calculated by using a full potential linearized augmented plane wave (LAPW) method with the local density approximation for the exchange-correlation potential. We used the program codes TSPACE (Ref. 23) and KANSAI-03. The scalar relativistic effects were taken into account for all electrons, and the spin-orbit interactions were included self-consistently for all valence electrons in a second variational procedure.

The lattice parameters used for the calculations were $a=10.1525$ Å and $x=0.3146$ for the $48f$ sites of oxygen.[13] The muffin-tin (MT) radii were set as $0.117a$ for Cs and Os, and $0.060a$ for O. Core electrons (Kr core for Cs, Xe core minus $5p^6$ for Os, and He core for O) were calculated inside the MT spheres in each self-consistent step. The $4d^{10}$ electrons on Cs and the $5p^64f^{14}$ electrons on Os were treated as valence electrons by using a second energy window.

The LAPW basis functions were truncated at $|\mathbf{k}+\mathbf{G}_i| \leq 13.08(2\pi/a)$, corresponding to 2397 LAPW functions at the Γ point. The sampling points were uniformly distributed in the irreducible (1/48)th of the Brillouin zone; 231 $\mathbf{k}$ points (divided by 12, 12, 12) were used both for the potential convergence and for the final band structure.

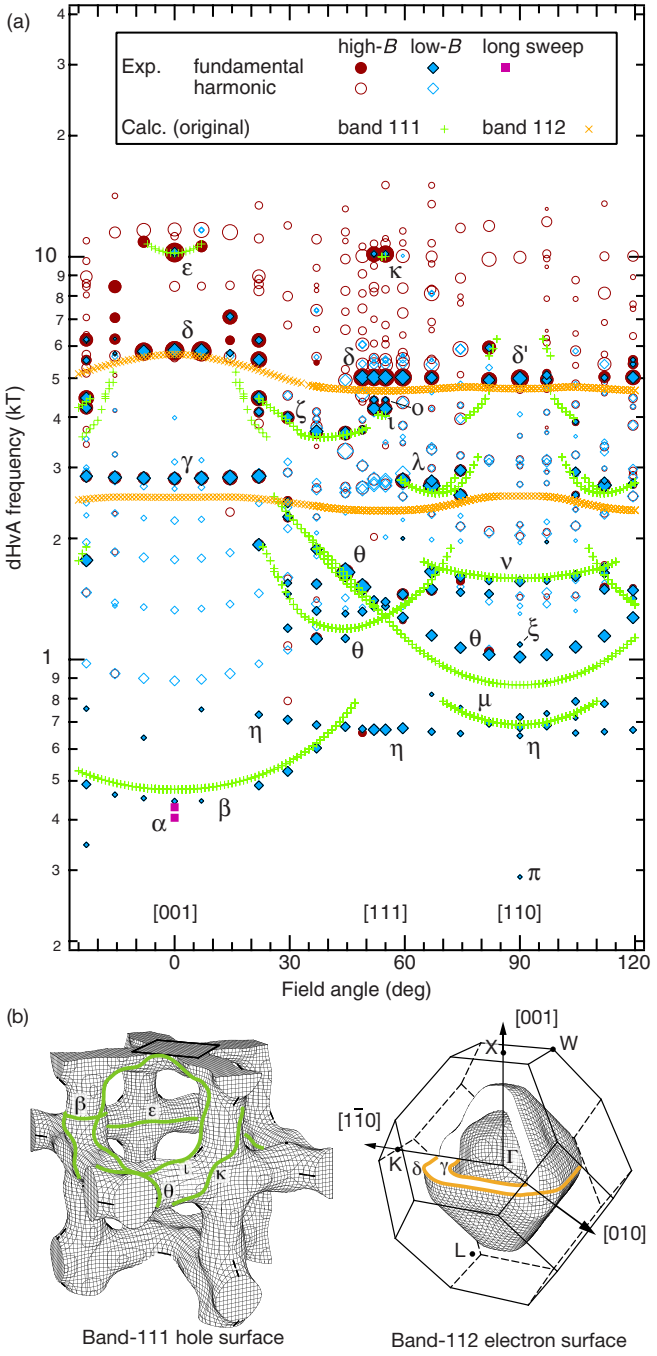

FIG. 4. (Color online) (a) Angular dependence of dHvA frequencies. The circles and diamonds denote experimental frequencies determined from the high-field and low-field sweeps, respectively. Fundamental frequencies are shown by filled symbols, while harmonics by open symbols. The sizes of the symbols are based on the amplitudes of dHvA oscillations. The squares indicate frequencies determined from the special long field sweeps. The Greek letters indicate the names of the frequency branches. The small + and × marks show frequencies predicted by the band-structure calculations, which yield the Fermi surface shown in (b). (b) The Fermi surface resulting from the original (unadjusted) band-structure calculations. Cyclotron orbits responsible for some of the frequency branches are also indicated. The band-112 surface consists of the two disconnected sheets, in between which electrons reside, and "dimples" appear in the ⟨111⟩ directions.

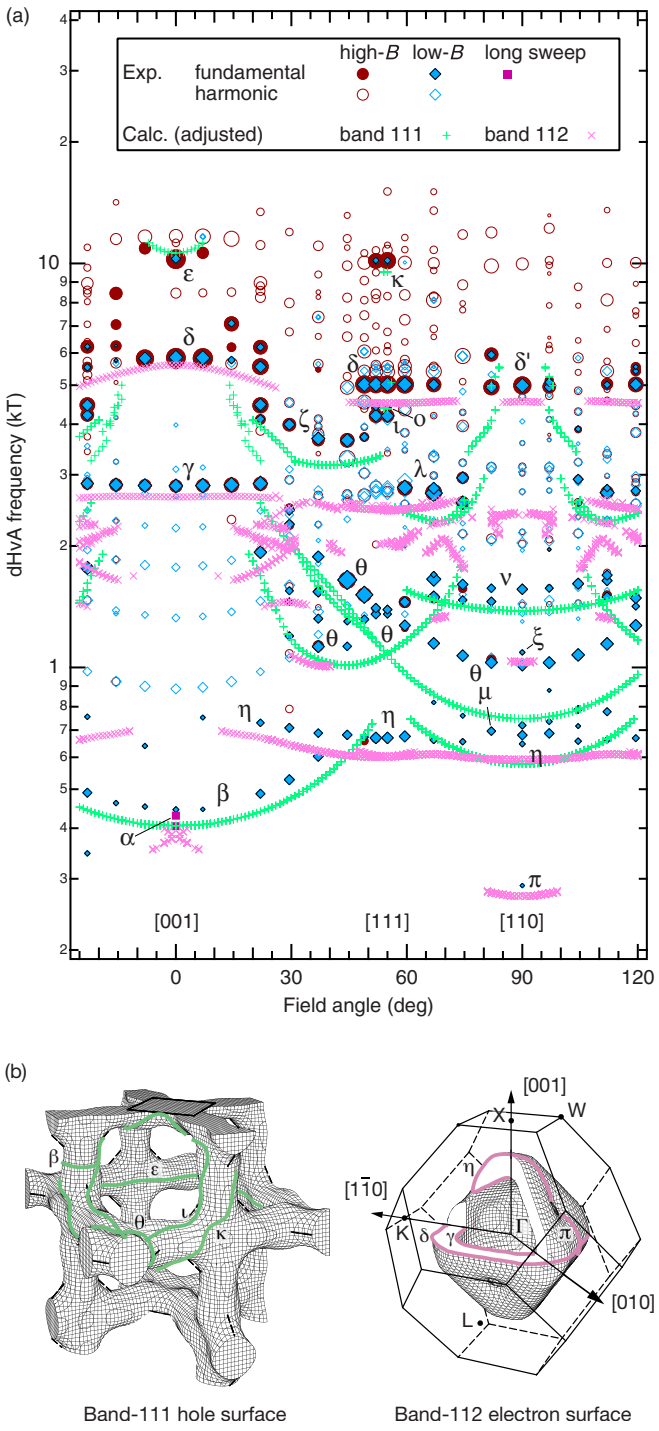

FIG. 5. (Color online) (a) The experimental data are the same as in Fig. 4. The calculated frequencies are based on the Fermi surface shown in (b), which gives the correct topology. (b) The adjusted Fermi surface. To obtain this Fermi surface, the bands are slightly shifted in energy, while the charge neutrality is kept (see text). The inner and outer sheets of the band-112 surface are connected, and through holes appear in the ⟨111⟩ directions.

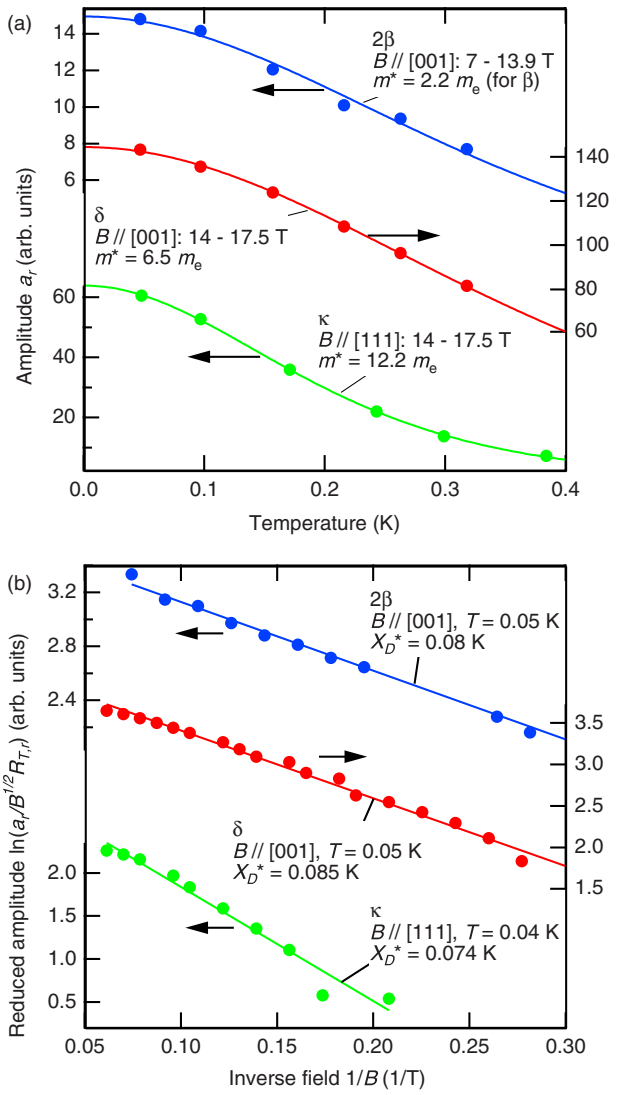

FIG. 6. (Color online) dHvA oscillation amplitudes (a) against temperature at constant fields and (b) against inverse field at constant temperatures. Orbit, field direction, and field range or temperature are given in the figures. The solid curves are fits based on Eq. (2), and estimated effective masses m^* or Dingle temperatures x_D^* are also shown in the figures.

III. RESULTS AND DISCUSSION

A. Upper critical field

The upper critical field B_{c2} was determined from ac magnetic susceptibility as shown in Fig. 2. $B_{c2}(0)$ is estimated at 1.4 T. Assuming that this is the orbital limiting field, we may estimate the coherence length ξ to be 15 nm.

B. de Haas–van Alphen measurements

We performed two field sweeps at each field direction: one from B=7 to 13.9 T, and the other from 14 to 17.5 T. We show Fourier transforms of dHvA oscillations in high symmetry directions, [001], [111], and [110], in Fig. 3. The spectra of the low-field sweeps (solid lines in Fig. 3) have a higher frequency resolution because of the wider $1/B$ range used, and also low-frequency oscillations are generally easier to see in the low-field spectra as explained above. On the other, the high-field spectra (dotted lines in Fig. 3) show high-frequency oscillations more clearly. We note that these spectra are rich in harmonic content, which is an indication

TABLE I. Experimental and calculated Fermi surface parameters.

Field direction	Branch	Orbit[a]	Experiment				Calculation				
							Unadjusted		Adjusted		
			F (kT)	m^*/m_e	x_D^* (K)	l (μm)	F (kT)	m_{band}/m_e	F (kT)	m_{band}/m_e	m^*/m_{band}
[001]	α_1[b]	(gp^e_{112})	0.41						(0.38)	(1.6)	
	α_2[b]	(gp^e_{112})	0.43						(0.39)	(1.7)	
	β[c]	W^h_{111}	0.45	2.2(2)	0.080(9)	0.93(5)	0.48	0.56	0.41	0.52	4.2
	γ	Γ^h_{112}	2.81	7.0(5)	0.088(6)	0.71(3)	2.53	1.96	2.65	2.05	3.4
	δ	Γ^e_{112}	5.85	6.5(2)	0.085(6)	1.05(5)	5.73	1.95	5.61	1.99	3.3
	ε	Γ^e_{111}	10.25	10.2(3)	0.080(6)	0.95(6)	10.20	3.11	10.61	3.18	3.2
[111]	η	gp^e_{112}	0.67	6.0(5)	0.12(2)	0.28(2)			0.60	2.00	3.0
	θ_1[c]	X^h_{111}	1.35	4.8(3)			1.28	1.57	1.08	1.46	3.3
	θ_2[c]	X^h_{111}	1.38	4.7(2)			1.28	1.57	1.08	1.46	3.2
	θ_3[c]	X^h_{111}	1.40	4.6(2)			1.28	1.57	1.08	1.46	3.2
		Λ^h_{112}							2.03	2.85	
		Γ^h_{112}					2.34	1.96	2.46	2.19	
	ι	L^e_{111}	4.20	9.2(3)	0.072(7)	0.75(6)	4.03	2.40	4.38	3.03	3.0
	o		4.42								
	δ	Γ^e_{112}	5.02	9.6(4)	0.079(7)	0.72(5)	4.65	2.26	4.51	2.44	3.9
	κ	L^h_{111}	10.15	12.2(5)	0.074(9)	0.85(8)	10.00	3.54	9.53	3.98	3.1
[110]	π	Σ^e_{112}	0.29						0.27	1.14	
	η	Δ^e_{112}	0.65						0.60	1.85	
	μ_1	gp^h_{111}	0.68	3.4(2)			0.69	0.91	0.58	0.81	4.3
	μ_2	gp^h_{111}	0.72	3.8(3)			0.69	0.91	0.58	0.81	4.8
	θ	X^h_{111}	1.02	3.6(2)	0.083(7)	0.81(5)	0.87	0.96	0.75	0.86	4.2
	ξ	gp^e_{112}	1.09						1.03	3.4	
	ν	S^h_{111}	1.56	6.6(2)			1.59	1.68	1.38	1.55	4.3
	δ'	Σ^e_{112}	4.99	11.4(3)	0.072(7)	0.66(5)	4.71	2.77	4.55	2.88	4.0

[a]Orbit assignments are based on the adjusted Fermi surface [Fig. 5(b)] and are denoted by orbit center, band number, and orbit character, i.e., electron or hole. "gp" is an abbreviation for a general point.

[b]According to the band-structure calculations, the α frequency does not exist for exactly $B\|$ [001]. Calculated values are those for the field direction 1° off the [001] axis.

[c]Experimental values are estimated from the second dHvA harmonic.

of a good sample quality. For the high symmetry directions, special long field sweeps were also performed to resolve finely split low frequencies as shown in the insets. The angular dependence of dHvA frequencies is shown in Figs. 4 and 5.

We estimated effective masses and Dingle temperatures associated with orbits for the symmetry directions as exemplified in Fig. 6, and the obtained values are summarized in Table I. We have also calculated electron mean free paths. The obtained values are close to 1 μm for most of the orbits (Table I). This confirms the very high quality of the sample, and the comparison of the mean free paths to the coherence length shows that the superconductivity in single-crystal $CsOs_2O_6$ is in the clean limit. The reason for the relatively short mean free path of η ($B\|[111]$) is not clear. We also examined the field dependence of the effective masses, but no significant dependence was found (Fig. 7).

C. Band-structure calculations and the Fermi surface

In Fig. 8, we show the calculated energy band structure near the Fermi level, which is similar to previously reported ones.[10–12] As can be seen from the total and partial densities of the states shown in Fig. 9, these 12 bands are mostly of Os 5d and O 2p characters. $CsOs_2O_6$ is a compensated metal, and two bands, 111 and 112, cross the Fermi level. As previously noted,[10] band-112 only slightly dips below the Fermi level along the ΓL line, giving rise to a van Hove singularity very close to the Fermi level. The two bands form the Fermi surface shown in Fig. 4(b). The existence of the van Hove singularity is manifested in the band-112 electron surface as "dimples" in the ⟨111⟩ directions. The density of states at the Fermi level is estimated at 63.4 states/Ry f.u. Theoretical dHvA frequencies calculated from this Fermi surface model are compared with the measured ones in Fig. 4(a), and also listed in Table I for the high symmetry directions together

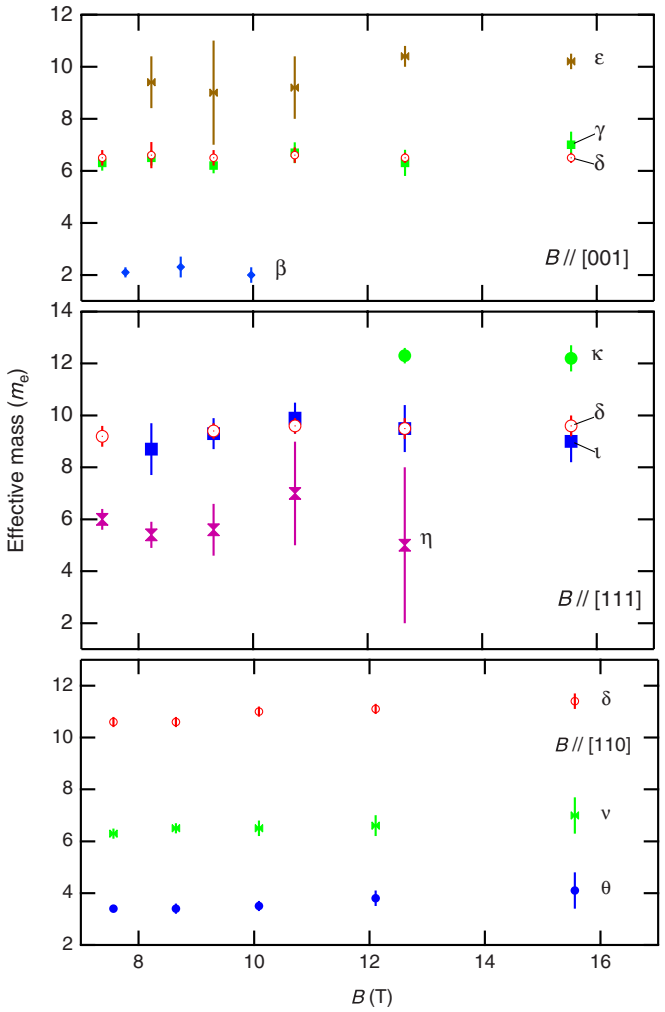

FIG. 7. (Color online) Effective masses as functions of magnetic field.

with calculated band masses. It can be seen that most of the experimental frequency branches are explained by this original (unadjusted) Fermi surface. Cyclotron orbits responsible for some of the branches are depicted in Fig. 4(b).

We, however, note the following discrepancies: (1) The δ frequency branch, which is assigned to a Γ-centered orbit on the band-112 surface [Fig. 4(b), right], is not observed experimentally around $\theta=35°$. (2) The η branch observed for a wide range of field angle cannot be explained. The former seems to relate with the fact that for $\theta=35°$, the cyclotron orbit responsible for δ would pass the dimples and suggests the existence of through holes in the $\langle 111 \rangle$ directions rather than the dimples.

Accordingly, we tried some adjustments by shifting each band in energy while keeping the carrier compensation. In Fig. 5(b), we show the Fermi surface obtained by lowering band 111 by 1.1 mRy and raising band 112 by 0.5 mRy. This reduces the carrier concentration from 0.326 to 0.281 electron/primitive cell, while the density of states becomes 64.3 states/Ry f.u. The van Hove singularity is now above the Fermi level, and through holes but not dimples occur in the $\langle 111 \rangle$ directions of the band-112 surface.

dHvA frequencies calculated from this adjusted Fermi surface are compared with the measured ones in Fig. 5(a). The absence of the δ frequency near $\theta=35°$ is explained well. The η branch can be explained by an orbit traversing two holes on the band-112 surface [Fig. 5(b), right]. Further, the α, π, and ξ frequencies are also attributed to orbits involving the holes of the band-112 surface. The ξ orbit is one connecting holes in the [111] and $[11\bar{1}]$ directions. According to the calculations, the α frequency, which arises from an orbit connecting holes in the [111] and $[1\bar{1}1]$ directions, does not occur for exactly $B\|[001]$, but appears as a doublet as soon as B is tilted. The experimental observation of two close frequencies α_1 and α_2 for $B\|[001]$ can be ascribed to a slight misorientation of the sample. These successful assignments of the experimental frequencies indicate that the adjusted Fermi surface describes the correct topology of the Fermi surface.

It, however, gives poorer agreement of the dHvA frequencies with experiment than the original one. Taking large orbits, for example, the frequencies ε and κ calculated from the original Fermi surface are in virtually perfect agreement with the measured ones [Fig. 4(a)], while in the case of the adjusted Fermi surface model, the calculated ε and κ frequencies are larger and smaller, respectively, than the measured ones [Fig. 5(a)]. Another example is θ: The measured θ frequency is 1.02 kT for $B\|[110]$. The original Fermi surface gives the value of 0.87 kT, while the adjusted one 0.75 kT, a still smaller value. As can be understood from Fig. 5(b), when tubes of the band-111 surface thin, orbits for κ and θ shrink, but that for ε expands. Hence, these discrepancies indicate that the carrier concentration was reduced too much in the adjusted Fermi-surface model. Turning to the band-112 surface, the calculated δ and γ frequencies are both smaller than the measured ones [Fig. 5(a)]. This again suggests that the carrier concentration is reduced too much. In order to improve agreement between theory and experiment, *both* the inner and outer sheets of the band-112 surface have to be expanded. Such adjustment can, however, not be achieved by a rigid band shift, which generally shifts the inner and outer sheets in opposite directions: See the band structure in Fig. 8. Band 112 dips the Fermi level near the middle of the ΓK line, for example. If the band is lowered, the outer sheet will expand, while the inner will shrink.

To summarize this section, the adjusted Fermi-surface model gives the correct topology of the Fermi surface. For $CsOs_2O_6$, the van Hove singularity is above the Fermi level unlike previously thought.[10–12] For quantitative improvement of the model, non-rigid-band effects would have to be considered.

D. Mass enhancement and Stoner enhancement

In this section, we consider the relative importance of electron-electron and electron-phonon mechanisms in many-body interactions in $CsOs_2O_6$.

Table II compares the enhancement of the electronic specific heat and magnetic susceptibility in $CsOs_2O_6$ with those in various compounds. The compounds listed are the strong-coupling superconductors Pb and Nb, the strongly enhanced paramagnet Pd, the nearly ferromagnetic metal Ni_3Ga, and the intermediate-valent compound $CeSn_3$. The ratio

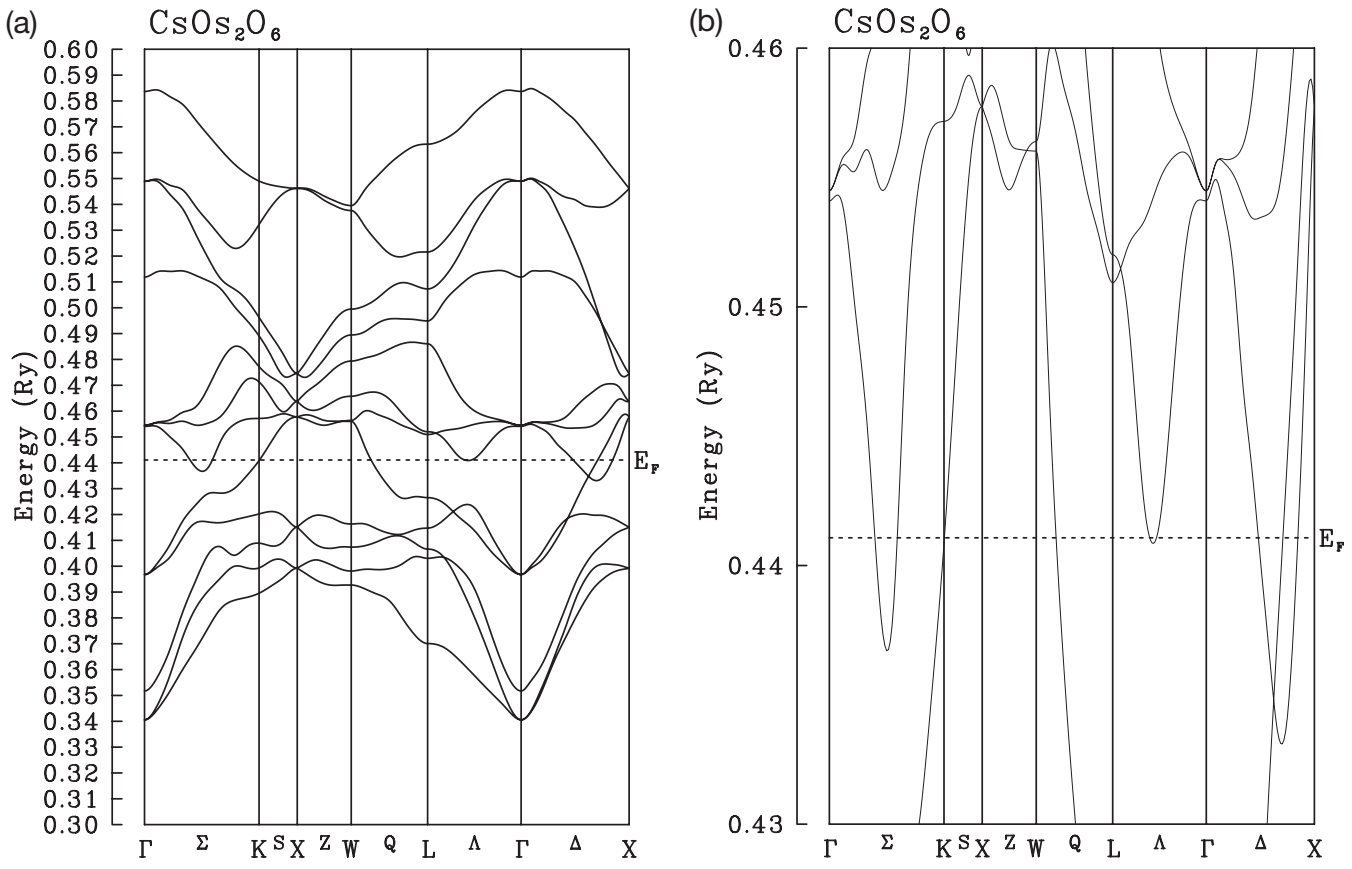

FIG. 8. (a) Calculated band structure of $CsOs_2O_6$ near the Fermi level E_F. (b) An enlarged view around E_F. E_F is at 0.441 069 Ry.

$\gamma_{exp}/\gamma_{band}$ is the specific-heat mass enhancement, to which both the electron-electron and electron-phonon interactions contribute. On the other hand, χ^c_{exp}/χ_{band} gives an estimate of the Stoner enhancement factor S, which stems only from the electron-electron interactions.[55] The ratio of the two ratios, namely, R in the last column, approximately gives the Wilson ratio: $R \approx S/[(1+\lambda_{ee})(1+\lambda_{ep})]$, where λ_{ee} and λ_{ep} are the electron-electron and electron-phonon mass enhancement factors, respectively. In general, $S/(1+\lambda_{ep}) > 1$ for the electron-electron interactions.[39] Hence, significant electron-phonon interactions are necessary to have R smaller than 1. Indeed, R is larger than 1 for all the compounds except $CsOs_2O_6$ and Pb. $R > 2$ even in Nb, in which the superconductivity is dominated by the electron-phonon interactions. In the case of $CeSn_3$, prevailing magnetic interactions are not necessarily ferromagnetic, unlike in Ni_3Ga; nevertheless, $R \sim 3$. The comparison shown in Table II, thus, clearly suggests the rather limited importance of the electron-electron interactions in $CsOs_2O_6$.

Since the Stoner enhancement factor S appears in the spin-splitting factor $R_{s,r}$ [Eq. (5)], orbit-specific values of S, or exactly the product Sg, can in favorable circumstances be determined for some orbits from dHvA data. According to Eq. (2), the amplitude a_r of the rth dHvA harmonic basically decreases exponentially with r. However, if many harmonics are observed, the oscillation as a function of r of the amplitude due to $R_{s,r}$ may be detected. Figure 10(a) shows the amplitudes of the β frequency and its harmonics for $B \| [001]$ against the harmonic number r. The amplitude is not monotonic, but clearly oscillates. The two solid curves are fits based on Eq. (2). We have used the values of $\mu^* = m^*/m_e = 2.2$ and $x_D = 0.080$ K determined above from the temperature and field dependences, respectively, and $m_{band}/m_e = 0.52$ from the adjusted calculation (Table I). Hence, there is only one free parameter, Sg, for these fits except for an overall proportionality factor. The curves correspond to $Sg = 1.682$ and 2.164, respectively. Because of the nature of the cosine function, the following series of values gives fits of the same quality: $Sg = 1.682 + 3.846n$ and $2.164 + 3.846n$, where $n = 0, 1, 2, \ldots$.

When the spin-orbit coupling is operative, g can be different from the free-electron value $g = 2$. However, appreciable deviations can occur only for very small orbits located at Brillouin zone boundaries, e.g., the Zn needle orbit with $F = 1.5$ T.[22] Since the β orbit is not so small, g is not very much different from 2. As mentioned above, the Fermi-surface average of S is about 3.1. Accordingly, in the following, we consider only Sg values corresponding to $n \leqslant 2$ in the above series.

We note that at $\theta = 14.5°$, the fundamental of β is not observed, while the second and higher harmonics are observed [see Fig. 4(a) or 5(a)]. This is a phenomenon called a spin-splitting zero, namely, $R_{s,r} = 0$ for a particular frequency and a particular field direction.[22] Figure 10(b) shows the amplitude of β as a function of the field angle. We can calculate the spin-splitting factor $R_{s,1}$ for the values of Sg under consideration, using the band mass. The results are shown together. It is clear that $Sg = 5.528$ or 9.374 for a spin-splitting

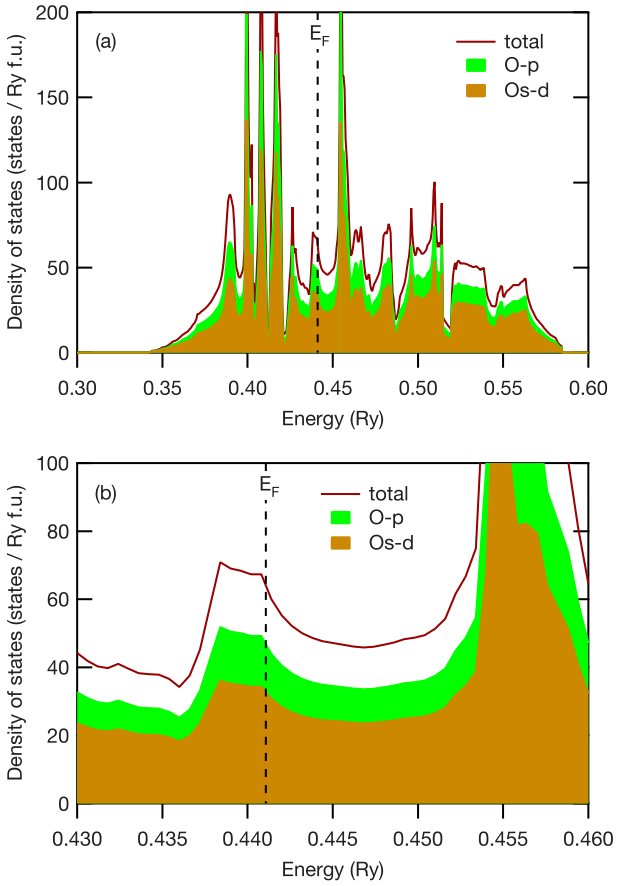

FIG. 9. (Color online) (a) Calculated total and partial densities of states for $CsOs_2O_6$ near the Fermi level E_F. (b) An enlarged view around E_F.

zero to occur near $\theta=15°$. The latter, 9.374, seems more compatible with the observed angular dependence of the amplitude. Then Fig. 10(c) shows the amplitude of the second harmonic together with $R_{s,2}$ for the two values of Sg. The value of 9.374 again appears more suitable to explain a sudden drop of the amplitude between $\theta=14.5$ and 22°.

If we assume $g=2$, $Sg=9.374$ means $S=4.7$. This estimate as well as the Fermi-surface average of $S\sim3.1$ is slightly larger than previous band-structure predictions, 2.57 (Ref. 10) and 2.15 (Ref. 11) for KOs_2O_6. However, they are still comparable to the value in the phonon-mediated superconductor Nb, and are far from suggesting strong electron correlations in $CsOs_2O_6$.

Our negative conclusion about the dominance of the electron-electron interactions in $CsOs_2O_6$ is in line with previous band-theoretical analyses on AOs_2O_6.[10–12] It is also in agreement with a conclusion from specific-heat measurements on $RbOs_2O_6$: it has been concluded in Ref. 9 that $RbOs_2O_6$ is a phonon-mediated superconductor. On the other hand, there are some reports[15,20] suggesting stronger electron correlations in KOs_2O_6. In this connection, we note that band-structure calculations indicate that the position of the van Hove singularity moves downward in energy as one moves from A=Cs through Rb to K.[12,13] Therefore, the position of the singularity may be very close to the Fermi level in KOs_2O_6. This might lead to stronger electron-electron interactions in the K compound. It will be interesting to experimentally investigate the position of the singularity, namely, whether it is above or below the Fermi level, in the Rb and K compounds.

Last, we return to Table I. The values of the dHvA mass enhancement m^*/m_{band} are mostly between 3 and 4, which is consistent with the specific-heat mass enhancement of 3.6 (Table II). It is tempting to argue that the observed nearly homogeneous mass enhancement over the Fermi surface, i.e., momentum-independent enhancement, is a signature of enhancement due to electron–rattling-phonon interactions because the rattling vibration is a local vibration in essence. However, this argument is simplistic.

Figure 11 shows a plot of dHvA mass enhancement vs frequency for various compounds. The compounds shown are the same as in Table II except for Nb, plus the recently discovered heavy-fermion $PrOs_4O_{12}$, the mechanism of whose mass enhancement is not clear, and the representative heavy-fermion compounds $CeRu_2Si_2$ and UPt_3. The form of enhancement vs frequency is based on the following expec-

TABLE II. Enhancement of the electronic specific heat and magnetic susceptibility in $CsOs_2O_6$ (experimental values are from Refs. 8 and 21) compared with those in Pb (Refs. 24–26), Nb (Refs. 27–29), Pd (Refs. 30–32), Ni_3Ga (Refs. 33–35), and $CeSn_3$ (Refs. 36 and 37). $\chi^c_{exp}=\chi_{exp}+|\chi_{core}|$, where χ_{exp} is the experimental low-temperature susceptibility, and χ_{core} the diamagnetic susceptibility of ion cores. Values of χ_{core} were estimated from literature values (Ref. 38). $R=(\chi^c_{exp}/\chi_{band})/(\gamma_{exp}/\gamma_{band})$.

	DOS $\left(\frac{\text{states}}{\text{Ry f.u.}}\right)$	γ_{exp} $\left(\frac{\text{mJ}}{\text{K}^2\,\text{mol}}\right)$	γ_{band} $\left(\frac{\text{mJ}}{\text{K}^2\,\text{mol}}\right)$	$\gamma_{exp}/\gamma_{band}$	χ^c_{exp} $\left(10^{-4}\,\frac{\text{emu}}{\text{mol}}\right)$	χ_{band} $\left(10^{-4}\,\frac{\text{emu}}{\text{mol}}\right)$	χ^c_{exp}/χ_{band}	R
$CsOs_2O_6$	64.3	40	11.1	3.6	4.7	1.53	3.1	0.86
Pb	7.4	3.0	1.3	2.3	0.06	0.18	0.3	0.14
Nb	28.2	7.8	4.88	1.6	2.52	0.670	3.76	2.3
Pd	32.7	9.42	5.67	1.66	7.6	0.777	9.8	5.9
Ni_3Ga	84.8	40 or 24[a]	14.7	2.7 or 1.6[a]	165	2.01	82	30 or 51[a]
$CeSn_3$	89	65	15	4.3	25	2.1	12	2.8

[a]Because of an anomalous contribution to the specific heat at low temperatures, the determination of γ_{exp} in Ni_3Ga is not straightforward. Thus, two estimations based on temperature ranges $1\leqslant T\leqslant 5$ K and $10\leqslant T\leqslant 15$ K are shown (Refs. 33 and 34).

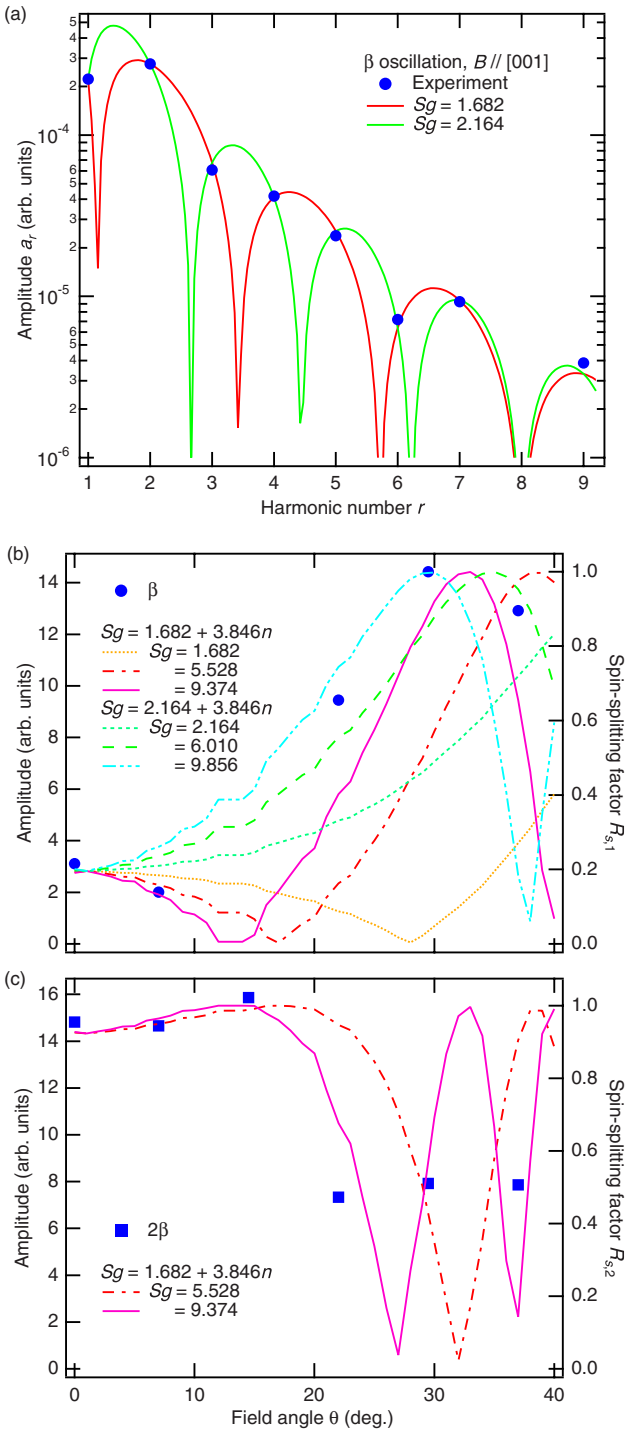

FIG. 10. (Color online) (a) Amplitudes of the β frequency and its harmonics as a function of the harmonic number for $B\|[001]$. The solid curves are fits based on Eq. (2), which gives the values of Sg shown in the figure. Amplitude of (b) the β frequency and (c) that of the second harmonic as functions of the field angle. The solid curves are the spin-splitting factor calculated from the values of Sg shown in the figure and the band mass.

tation: Although mass enhancements determined for small orbits may deviate largely because they represent only a small part of the Fermi surface, those for large orbits will converge on the specific-heat mass enhancement. This expectation is more or less correct except for $PrOs_4Sb_{12}$ and

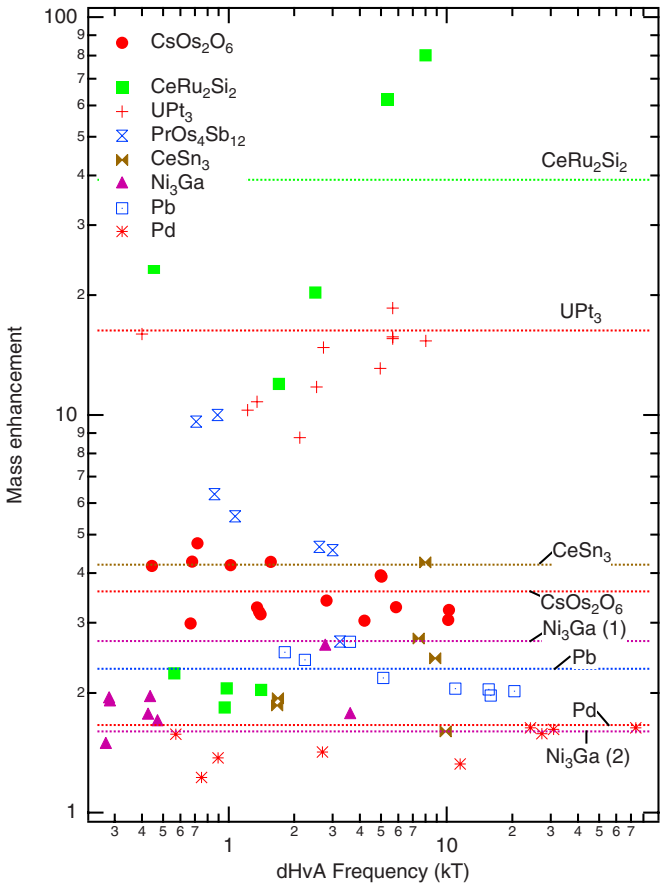

FIG. 11. (Color online) Mass enhancement in $CsOs_2O_6$ in comparison with those in Pd (Refs. 30, 31, 40, and 41), Pb (Refs. 24, 25, and 42), Ni_3Ga (Refs. 33 and 34), $CeSn_3$ (Refs. 36 and 43), $PrOs_4Sb_{12}$ (Refs. 44 and 45), UPt_3 (Refs. 46–48), and $CeRu_2Si_2$ (Refs. 49–54). The marks show dHvA mass enhancement m^*/m_{band} against dHvA frequency, while the horizontal dotted lines indicate specific-heat mass enhancement $\gamma_{exp}/\gamma_{band}$. For Ni_3Ga, both the low-T and the high-T estimation are shown (see the footnote of Table II). For $PrOs_4Sb_{12}$, the specific-heat mass enhancement is not shown because of difficulty in determination of γ_{exp} (Ref. 45).

$CeRu_2Si_2$. The scatter of enhancements for different orbits is of similar magnitude, a factor of 2 or less, for all the other compounds despite different mechanisms of mass enhancement. Thus, the homogeneous enhancement observed for $CsOs_2O_6$ is, unfortunately, not necessarily a signature of the electron-rattling interactions.

IV. SUMMARY

We have performed detailed dHvA measurements and band-structure calculations for $CsOs_2O_6$. By comparing the experimental angular dependence of dHvA frequencies with the calculated one, we have found that the topology of the Fermi surface can be described by the band-structure calculations if slight rigid band shifts are incorporated. Band-112 electron surface has through holes in the ⟨111⟩ directions instead of the dimples previously suggested. This means that the van Hove singularity is above the Fermi level in $CsOs_2O_6$, contrary to the previous thoughts.[10–12]

We have estimated that the Stoner enhancement factor $S \sim 3.1$ and that the Wilson ratio $R \sim 0.86$, by comparing experimental susceptibility and Sommerfeld coefficient with band-structure results. The dHvA mass enhancement ranges approximately from 3 to 4, which is consistent with the specific-heat mass enhancement of 3.6. We have also estimated the orbit-specific Stoner enhancement factor for the β orbit: the analyses indicate most likely $Sg=9.374$. The small Wilson ratio and Stoner enhancement factor indicate rather limited importance of electron-electron interactions. It is unlikely that the electron-electron interactions prevail over the electron-phonon ones in $CsOs_2O_6$. This conclusion is in line with previous studies such as Refs. [9–12]. Since possible signs of stronger electron correlations have been reported for KOs_2O_6,[15,20] experimental determination of electronic band structures in the Rb and K compounds deserves further efforts.

Finally, we have considered implications of the observation that the mass is enhanced homogeneously over the Fermi surface, but it has turned out that the homogeneous mass enhancement itself cannot be regarded as an indication of the electron-rattling interactions.

ACKNOWLEDGMENTS

This work was supported by Grants-in-Aid for Scientific Research from the JSPS, Japan.

[1] S. Yonezawa, Y. Muraoka, Y. Matsushita, and Z. Hiroi, J. Phys.: Condens. Matter **16**, L9 (2004).
[2] S. Yonezawa, Y. Muraoka, Y. Matsushita, and Z. Hiroi, J. Phys. Soc. Jpn. **73**, 819 (2004).
[3] S. Yonezawa, Y. Muraoka, and Z. Hiroi, J. Phys. Soc. Jpn. **73**, 1655 (2004).
[4] Z. Hiroi, S. Yonezawa, J. Yamaura, T. Muramatsu, Y. Matsushita, and Y. Muraoka, J. Phys. Soc. Jpn. **74**, 3400 (2005).
[5] J. Yamaura, S. Yonezawa, Y. Muraoka, and Z. Hiroi, J. Solid State Chem. **179**, 336 (2006).
[6] R. Galati, R. W. Hughes, C. S. Knee, P. F. Henry, and M. T. Weller, J. Mater. Chem. **17**, 160 (2007).
[7] Z. Hiroi, S. Yonezawa, Y. Nagao, and J. Yamaura, Phys. Rev. B **76**, 014523 (2007).
[8] Z. Hiroi, S. Yonezawa, T. Muramatsu, J. Yamaura, and Y. Muraoka, J. Phys. Soc. Jpn. **74**, 1255 (2005).
[9] M. Bruhwiler, S. M. Kazakov, J. Karpinski, and B. Batlogg, Phys. Rev. B **71**, 214517 (2005).
[10] R. Saniz, J. E. Medvedeva, L.-H. Ye, T. Shishidou, and A. J. Freeman, Phys. Rev. B **70**, 100505(R) (2004).
[11] J. Kuneš, T. Jeong, and W. E. Pickett, Phys. Rev. B **70**, 174510 (2004).
[12] R. Saniz and A. J. Freeman, Phys. Rev. B **72**, 024522 (2005).
[13] Z. Hiroi, J. Yamaura, S. Yonezawa, and H. Harima, Physica C **460-462**, 20 (2007).
[14] Z. Hiroi, S. Yonezawa, and Y. Muraoka, J. Phys. Soc. Jpn. **73**, 1651 (2004).
[15] Y. Kasahara, Y. Shimono, T. Shibauchi, Y. Matsuda, S. Yonezawa, Y. Muraoka, and Z. Hiroi, Phys. Rev. Lett. **96**, 247004 (2006).
[16] T. Muramatsu, N. Takeshita, C. Terakura, H. Takagi, Y. Tokura, S. Yonezawa, Y. Muraoka, and Z. Hiroi, Phys. Rev. Lett. **95**, 167004 (2005).
[17] A. Koda, W. Higemoto, K. Ohishi, S. R. Saha, R. Kadono, S. Yonezawa, Y. Muraoka, and Z. Hiroi, J. Phys. Soc. Jpn. **74**, 1678 (2005).
[18] V. Keppens, D. Mandrus, B. C. Sales, B. C. Chakoumakos, P. Dai, R. Coldea, M. B. Maple, D. A. Gajewski, E. J. Freeman, and S. Bennington, Nature (London) **395**, 876 (1998).
[19] G. Schuck, S. M. Kazakov, K. Rogacki, N. D. Zhigadlo, and J. Karpinski, Phys. Rev. B **73**, 144506 (2006).
[20] M. Bruhwiler, S. M. Kazakov, J. Karpinski, and B. Batlogg, Phys. Rev. B **73**, 094518 (2006).
[21] Y. Nagao (unpublished).
[22] D. Shoenberg, *Magnetic Oscillations in Metals* (Cambridge University Press, Cambridge, England, 1984).
[23] A. Yanase, *Fortran Program for Space Group*, 1st ed. (Shokabo, Tokyo, 1985).
[24] J. R. Anderson, W. J. O'Sullivan, and J. E. Schirber, Phys. Rev. B **5**, 4683 (1972).
[25] B. J. C. van der Hoeven and P. H. Keesom, Phys. Rev. **137**, A103 (1965).
[26] W. D. Knight, in *Solid State Physics*, edited by F. Seitz and D. Turnbull (Academic, New York, 1956), Vol. 2, p. 114.
[27] J. R. Anderson, D. A. Papaconstantopoulos, J. W. McCaffrey, and J. E. Schirber, Phys. Rev. B **7**, 5115 (1973).
[28] F. Heininger, E. Bucher, and J. Muller, Phys. Kondens. Mater. **5**, 243 (1966).
[29] D. Hechtfischer, Z. Phys. B **23**, 255 (1976).
[30] O. K. Andersen, Phys. Rev. B **2**, 883 (1970).
[31] B. W. Veal and J. A. Rayne, Phys. Rev. **135**, A442 (1964).
[32] S. Foner, R. Doclo, and J. E. J. McNiff, J. Appl. Phys. **39**, 551 (1968).
[33] S. M. Hayden, G. G. Lonzarich, and H. L. Skriver, Phys. Rev. B **33**, 4977 (1986).
[34] W. de Dood and P. F. de Chatel, J. Phys. F: Met. Phys. **3**, 1039 (1973).
[35] C. J. Schinkel, F. R. de Boer, and B. de Hon, J. Phys. F: Met. Phys. **3**, 1463 (1973).
[36] A. Hasegawa, H. Yamagami, and H. Johbettoh, J. Phys. Soc. Jpn. **59**, 2457 (1990).
[37] J. K. A. Gschneidner, S. K. Dhar, R. J. Stierman, T. W. E. Tsang, and O. D. McMasters, J. Magn. Magn. Mater. **47&48**, 51 (1985).
[38] *Kagaku Binran Kiso-hen (Handbook of Chemistry)*, edited by The Chemistry Society of Japan, 4th ed. (Maruzen, Tokyo, 1993), Vol. II, p. 505.
[39] J. W. Wilkins, in *Electrons at the Fermi Surface*, edited by M. Springford (Cambridge University Press, Cambridge, England, 1980), p. 46.
[40] D. H. Dye, S. A. Campbell, G. W. Crabtree, J. B. Ketterson, N. B. Sandesara, and J. J. Vuillemin, Phys. Rev. B **23**, 462 (1981).
[41] B. Schmidt and E. Mrosan, Solid State Commun. **40**, 749 (1981).

[42] R. A. Phillips and A. V. Gold, Phys. Rev. **178**, 932 (1969).
[43] I. Umehara, Y. Kurosawa, N. Nagai, M. Kikuchi, K. Satoh, and Y. Ōnuki, J. Phys. Soc. Jpn. **59**, 2848 (1990).
[44] H. Sugawara *et al.*, Phys. Rev. B **66**, 220504(R) (2002).
[45] M. B. Maple, J. Phys. Soc. Jpn. **74**, 222 (2005).
[46] N. Kimura *et al.*, Physica B **281&282**, 710 (2000).
[47] P. H. Frings and J. J. M. Franse, Phys. Rev. B **31**, 4355 (1985).
[48] M. M. Steiner, R. C. Albers, and L. J. Sham, Phys. Rev. Lett. **72**, 2923 (1994).
[49] H. Aoki, S. Uji, A. K. Albessard, and Y. Ōnuki, Phys. Rev. Lett. **71**, 2110 (1993).
[50] F. S. Tautz, S. R. Julian, G. J. McMullan, and G. G. Lonzarich, Physica B **206-207**, 29 (1995).
[51] M. Takashita, M.S. thesis, University of Tsukuba, 1995.
[52] M. J. Besnus, J. P. Kappler, P. Lehmann, and A. Meyer, Solid State Commun. **55**, 779 (1985).
[53] J. D. Thompson, J. O. Willis, C. Godart, D. E. MacLaughlin, and L. C. Gupta, Solid State Commun. **56**, 169 (1985).
[54] H. Yamagami and A. Hasegawa, J. Phys. Soc. Jpn. **62**, 592 (1993).
[55] Although χ^{c}_{exp} has been corrected for the ion-core diamagnetism, since it still contains the paramagnetic Van Vleck term, this estimate is an approximation.